SEMIANNUAL TECHNICAL SUMMARY REPORT
FOR
HIGH-SPEED, LONG-WAVELENGTH COHERENT
RADIATION DETECTORS

R. L. Williams

Texas Instruments Incorporated

15 May 1967 through 15 November 1967

Contract N00014-?-C-0497

Department of the Navy
Office of Naval Research
Washington, D. C.

in cooperation with

Advanced Research Projects Agency
Department of Defense
Washington, D. C.

ARPA Order No. 269
Program Code No. 7E30

December 1967

TI Report No. 08-67-90

SEMIANNUAL TECHNICAL SUMMARY REPORT
FOR
HIGH-SPEED, LONG-WAVELENGTH COHERENT
RADIATION DETECTORS

R. L. Williams

ABSTRACT

The principal consideration in the heterodyne mode of signal detection is the influence of the local oscillator power on detector characteristics. It is shown that misalignment of the local oscillator signal can seriously degrade detection performance with the detector geometry presently used. For signals incident through transparent contacts, misalignment problems are removed. Characteristics of transparent contacts are reported.

It has been established that dielectric relaxation time constant effects occur above a certain electric field. These effects, as well as nonlinearities of signal and detector resistance changes, occur at fields for which the drift length of holes is comparable to the electrode separation. This has been shown to be valid by examining detectors having different thicknesses and material having a wide range of carrier lifetimes.

Mercury-doped germanium samples which have been subjected to gallium diffusions have larger activation energies than untreated material. This change has been identified with copper gettering by the gallium-diffused surface layer.

R. L. Williams

R. L. WILLIAMS, Project Scientist
Advanced Components Research
Laboratory

George R. Pruett

G. R. PRUETT, Project Manager
Advanced Components Research
Laboratory

W. J. Beyen by G R Pruett

W. J. BEYEN, Director
Advanced Components Research
Laboratory

SEMIANNUAL TECHNICAL SUMMARY REPORT
FOR
HIGH-SPEED, LONG-WAVELENGTH COHERENT
RADIATION DETECTORS

TABLE OF CONTENTS

SECTION		PAGE
I	GENERAL DETECTOR CONSIDERATIONS	1
	A. Special Detector Considerations for Detecting Coherent Radiation	1
	1. Influence of Local Oscillator Power	1
	2. Detector Design Considerations Related to the Directional Property of Coherent Radiation	2
	B. Alignment Requirements for Heterodyning	12
II	MATERIAL PROPERTIES	15
	A. Dielectric Relaxation Studies	15
	1. Introduction	15
	2. Experimental	15
	3. Discussion of Results	25
	B. Impurity Interactions	27
	1. Gettering of Copper with a Gallium-Diffused Layer	27
	2. Electronic Solubility Enhancement	27
	3. Pairing Solubility Enhancement	30
	4. Radioactive Copper	30
	REFERENCES	31

TABLE OF CONTENTS
(continued)

LIST OF ILLUSTRATIONS

FIGURE		PAGE
1	Conventional Detector Geometry with Coherent Radiation Incident "Normal" to the Electric Field	3
2	Collinear Detector Geometry with Coherent Radiation Incident Collinear with the Electric Field	5
3	Arrangement of Detectors with Transparent Contacts so that Normal and Collinear Modes of Operation Can Be Investigated During the Same Experimental Run	8
4	Normal and Collinear Spectral Response for a Gold-Gallium Alloy Contact	9
5	Normal and Collinear Spectral Response for a Gallium-Diffused Layer Contact	10
6	Falloff in Signal Response with Angular Misalignment of Signal and Local Oscillator Propagation Directions . .	14
7	Photographs of Oscilloscope Traces Showing the Change from Fast to Slow Signal Response as the Detector Bias Is Increased	16
8	Variation of A_p/A_f with Electric Fields for Detector Materials of Varying Sensitivities	17
9	Variation of A_p/A_f with Electric Field for Ge:Hg, Ge:Cu, and Mixed Ge:Hg:Cu Materials	19
10	Variation of the Field Dependence of the DR Effects with Electrode Separation	20
11	Variation of Current Responsivity i_s/V, Detector Resistance, and A_p/A_f with Electric Field	22
12	Variation of the Total Signal, 15 Hz, and the Fast Component, 15 kHz and 150 kHz, with Bias	24
13	Schematic Diagram of a Detector	26
14	Impurity Gettering with a Gallium-Diffused Layer	28
15	Solubility Enhancement due to Acceptors	29

TABLE OF CONTENTS
(continued)

LIST OF TABLES

TABLE		PAGE
I	Collinear and Normal Detector Response in a Signal Field of 1.2×10^{-5} Watt/Cm^2.	11

BLANK PAGE

SECTION I

GENERAL DETECTOR CONSIDERATIONS

A. Special Detector Considerations for Detecting Coherent Radiation

1. Influence of Local Oscillator Power

a. Background Radiation

Photodetectors operating in the 8 to 14 micron region are limited in performance by 300°K background radiation. Signal levels are much smaller than the 300°K background power density on the detector, i.e., much smaller than 5.0×10^{-3} watt/cm^2/2π steradians. Thus, resistance changes for such signals are small compared to the quiescent resistance value set by the background. Similarly, for the heterodyne mode of operation in which the local oscillator power will exceed 300°K background levels, the signal power will not significantly alter the operating conditions. For both coherent and noncoherent detection mechanisms, the signal falling on the same portion of the detector as the "background" will respond according to the average operating conditions determined by that background.

b. Power Considerations

For coherent detection the signal current is given by[1-4]

$$i_S = R(Q_{\ell o} Q_S)^{\frac{1}{2}} ,$$

where R is the current responsivity per photon, and $Q_{\ell o}$ and Q_S are the local oscillator and signal photon signals, respectively. Significant gain and heterodyning sensitivity limits are realized only when $Q_{\ell o} \gg Q_S$ and $Q_{\ell o}$ is greater than the 300°K background photon flux. Consequently, $\Delta n_S/n_{\ell o} \ll 1$ or to heterodyne implies small signal considerations. It then follows that for heterodyne detection, detector considerations are related to the effect $Q_{\ell o}$ has on the detector parameters. In this respect it is valuable to consider possible lifetime changes and the significance of the directional character of the coherent radiation.

c. Lifetime Changes

For example, consider a detector that will operate as fast as 1.0×10^{-9} seconds. The $Q_{\ell o}$ will be in the range 10^{18} to 10^{19} photons/sec/cm^2. Thus, for a depth of penetration t equal to 1 mm the carrier density $n = \eta Q_{\ell o}/t\tau = 10^9$ to 10^{10}/cc (efficiency η taken as 1). Because counter doping levels which control lifetime are 2 or 3 orders of magnitude greater than this, there will be little effect on lifetime as a result of the local oscillation signal. At the same time, for lifetime in the 10^{-6} sec range local oscillator power may well modify detector parameters.

2. Detector Design Considerations Related to the Directional Property of Coherent Radiation

a. Directional Property of Coherent Radiation

One feature of coherent radiation is its parallelism or its non-divergent character. By contrast, incoherent radiation from the 300°K background is random in direction. The consequence for detector operation can be considerable. Since the local oscillator signal originates outside the detector assembly, it has to be directed onto the detector.

In the series of illustrations in Figure 1, the results of misalignment of the local oscillator signal are detailed. Radiation covering only part b of the detector [Figure 1(a)] will give rise to a resistivity profile [Figure 1(b)]. Even when coherent detection is utilized, the 300°K background radiation will still be present. This sets the value ρ_a, while the smaller value ρ_b is determined by the combination of both radiation fluxes. Since sections a and b are in series, the equivalent circuit can be described as shown in Figure 1(c). The signal will be registered as a change of R_b or ΔR_b, while R_a is unaffected even if the signal falls on section a because no coherent radiation reference signal is present.

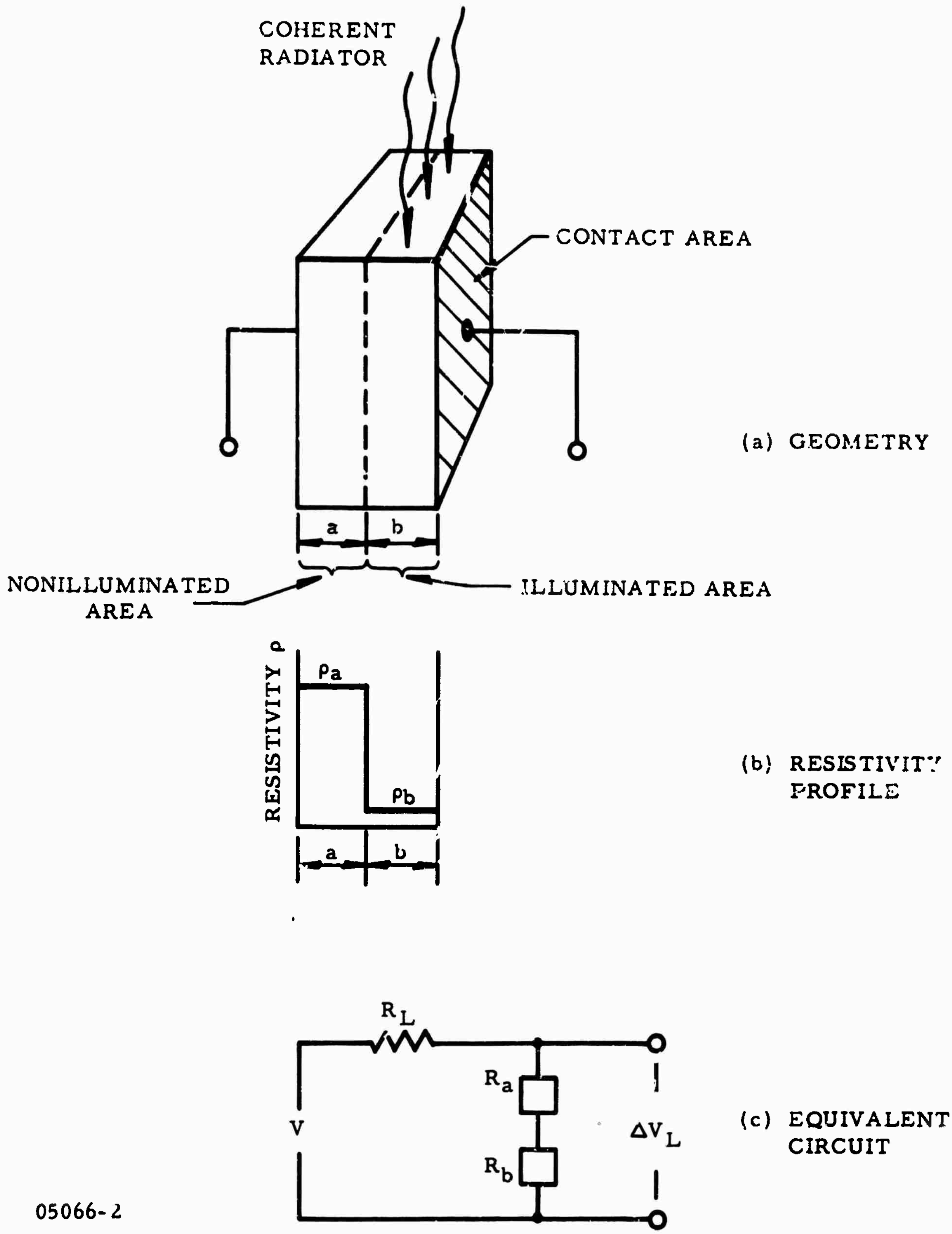

Figure 1 Conventional Detector Geometry with Coherent Radiation Incident "Normal" to the Electric Field. For the local oscillator radiation falling on a part of the detector (a), a blocking resistance develops (b) and (c), which reduces the responsivity of the detector.

For a bias voltage V impressed across the load resistor R_L, the signal voltage ΔV_L appearing across the load is given by the expression

$$\Delta V_L = \frac{R_L \ \Delta R_b \ I}{R_L + R_a + R_b} \ .$$

The direct current value is I. For high speeds of operation, R_L is smaller than R_a or R_b to reduce RC effects; thus, usually

$$\Delta V_L \approx \frac{R_L}{R_b} \ \Delta R_b I \ \frac{R_b}{R_a + R_b} \ .$$

The last factor, $R_b/R_a + R_b$, is a signal reduction caused by the blocking effect of R_a, which will be at least an order of magnitude greater than R_b. For variable background conditions R_b/R_a could have values resulting in serious signal loss variations.

While good system design might reduce the probability of such misalignment, an alternative configuration, shown in Figure 2, eliminates these effects.

b. <u>Transparent Contacts</u>

In the situation depicted in Figure 2, transparent contacts have been applied to the surface through which the radiation passes. Once again we consider a local oscillator signal falling only on part <u>b</u> of the detector; thus, the resistivity profile across the detector element will be the same as in Figure 1(b). However, for the contact configuration of 2(a) the appropriate equivalent circuit is that of 2(c) in which the illuminated and nonilluminated areas are parallel resistances.

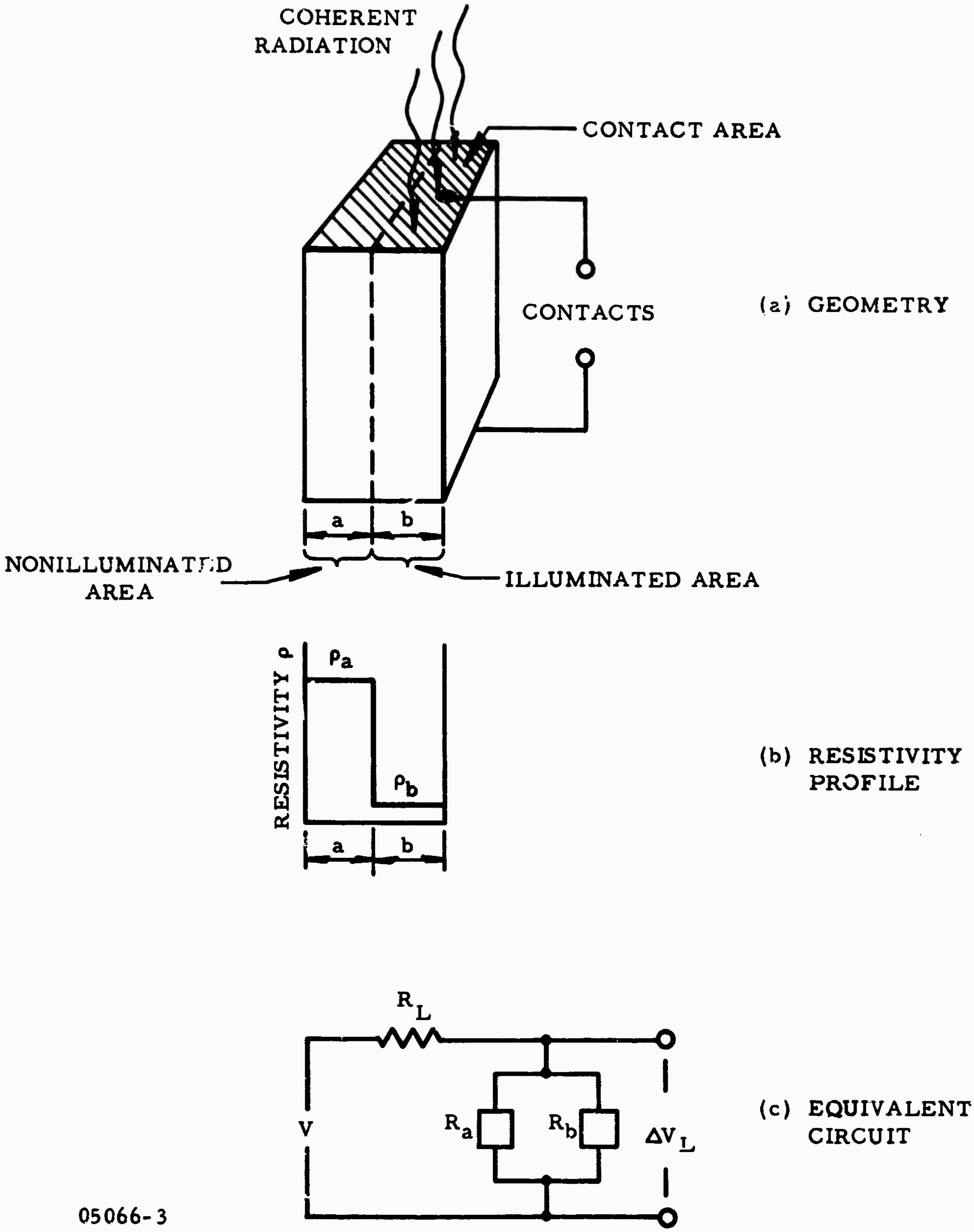

Figure 2 Collinear Detector Geometry with Coherent Radiation Incident Collinear with the Electric Field. For the local oscillator radiation falling on a part of the detector (a), no blocking resistance occurs (b) and (c).

For this case the signal voltage developed across the load resistor is

$$\Delta V_L = \frac{R_L I \Delta R_b}{\left(R_L + \frac{R_a R_b}{R_a + R_b}\right)} \left(\frac{R_a}{R_a + R_b}\right)^2 .$$

For the condition discussed in the previous case, i.e., $R_L < R_b$, R_a, the above expression reduces to

$$\Delta V_L = R_L I \Delta R_b \cdot \frac{R_a}{R_a + R_b} .$$

We see that for R_a 10 times R_b only a slight signal loss occurs, and for extreme situations $R_a \gg R_b$ the loss is negligible.

c. Collinear Mode of Operation

In the mode of operation described above the radiation is incident "collinear" with the device electric field, and in this "collinear" mode of operation blocking or saturation effects are absent. [In the conventional mode of operation, e.g., Figure 1(a), the radiation is "normal" to the electric field.]

d. Special Design Considerations Related to the Collinear Mode

Consider a detector material having a carrier lifetime τ of 10^{-9} sec and a hole mobility μ_p of 10^5 cm^2/V-sec. Then for an applied bias V of 10 volts across an element thickness t of 1 mm the gain $G = \tau\mu V/t^2$ has a value of 0.1. To achieve high gain or responsivity we require highest voltages of operation and thinnest electrode spacings. A discussion of bias effects will be presented in a subsequent section of this report; only the role of thickness will be considered here.

There are two conflicting collinear thickness requirements: (1) small values yield high gain, and (2) large values are needed for high absorption. At this point in the program the values of mercury concentrations in Ge:Hg are generally such that element thicknesses must be at least 1 mm or 2 mm to achieve adequate absorption. Increased Hg concentrations are very desirable for the optimum collinear mode detector operation.

e. Some Studies of the Collinear Mode

In the first phase of study of the collinear mode, some detectors with transparent contacts were made and the normal and collinear mode performances were compared. To do this, groups of four detectors, all having transparent contacts, were arranged on a mounting block as shown in Figure 3. In this configuration the spectral response and time constant measurements of the two forms can be immediately compared.

Figure 4 shows the spectral response of the two modes of operation utilizing a gold-gallium alloy contact, and Figure 5 shows spectral response for gallium diffused layers. It is apparent that no major difference occurs in the spectral response for the two modes of operation.

The long wavelength region has been emphasized as recent work has demonstrated that spectral response in this region can be related to secondary effects within the detector.[5]

Radiation losses occurring as the signal passes through the Au-Ga contact have been determined by comparing the current responsivity for the normal and collinear modes. Data taken on several samples are collected in Table I. The following features are apparent. The collinear mode $\Delta I/I$ values are always larger than the normal mode values. Characteristics obtained with the set of Ge:Cu detectors having a gallium diffused layer were similar to those of the Ge:Hg samples and a Au-Ga alloy layer. Detector

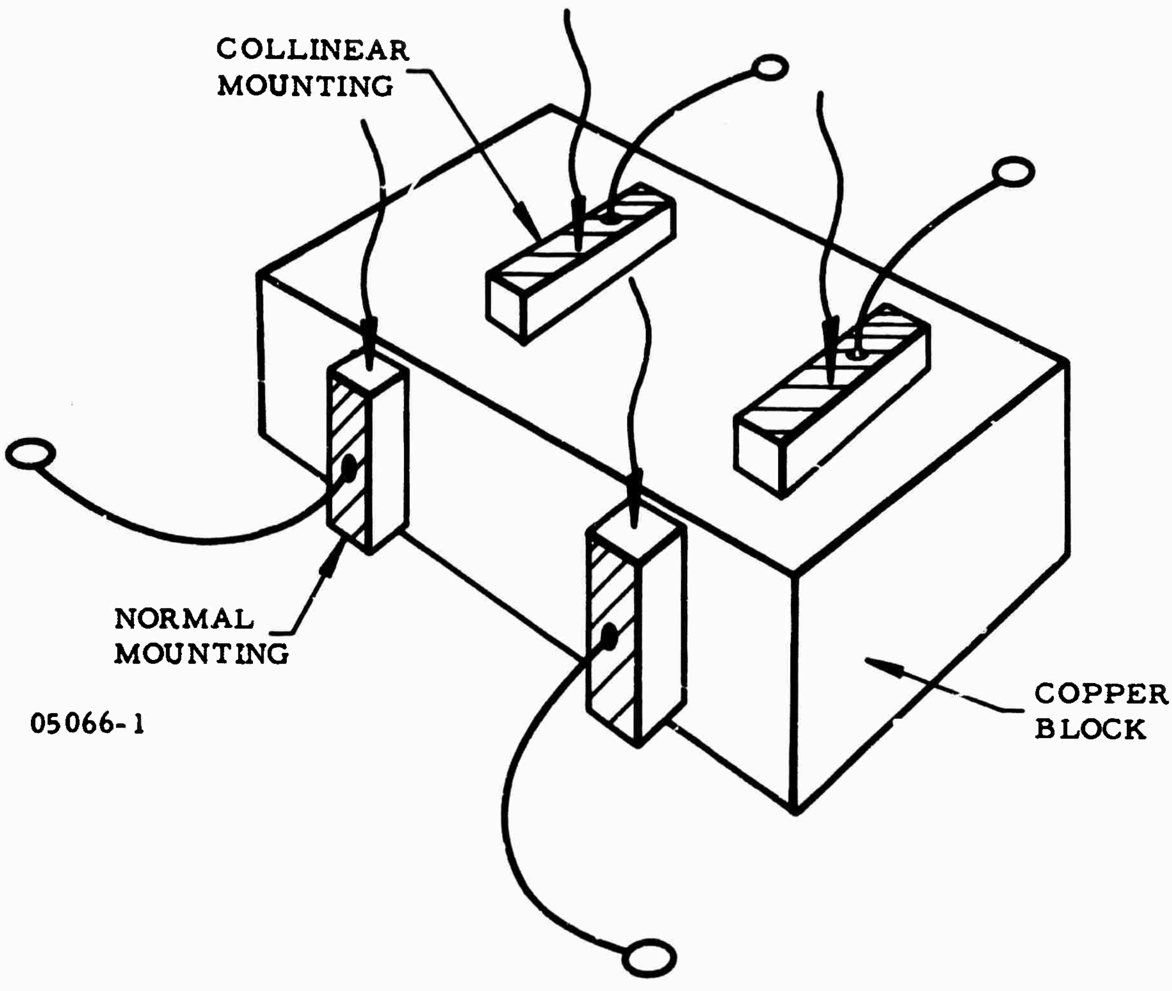

Figure 3 Arrangement of Detectors with Transparent Contacts so that Normal and Collinear Modes of Operation Can Be Investigated During the Same Experimental Run

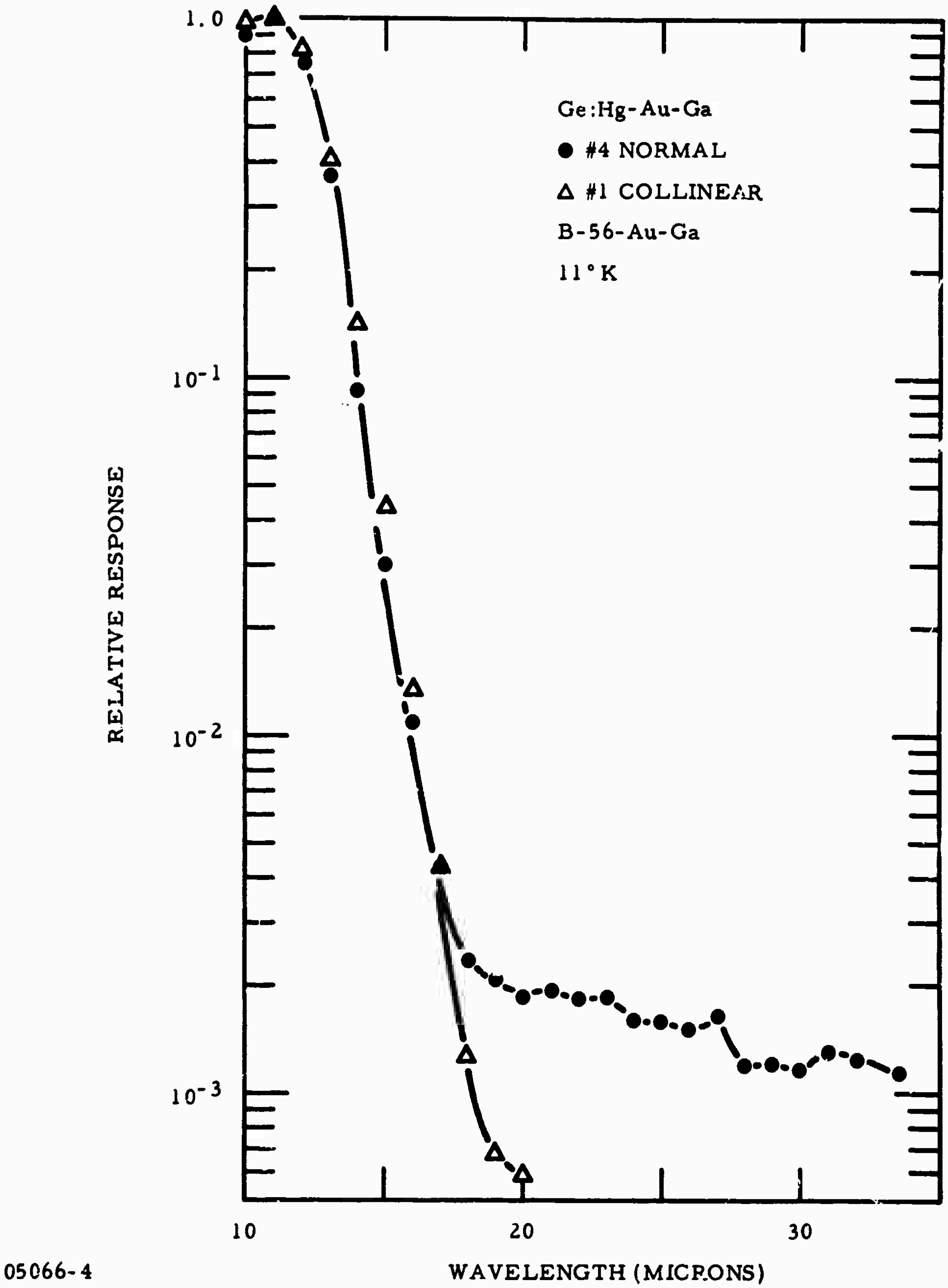

Figure 4 Normal and Collinear Spectral Response for a Gold-Gallium Alloy Contact

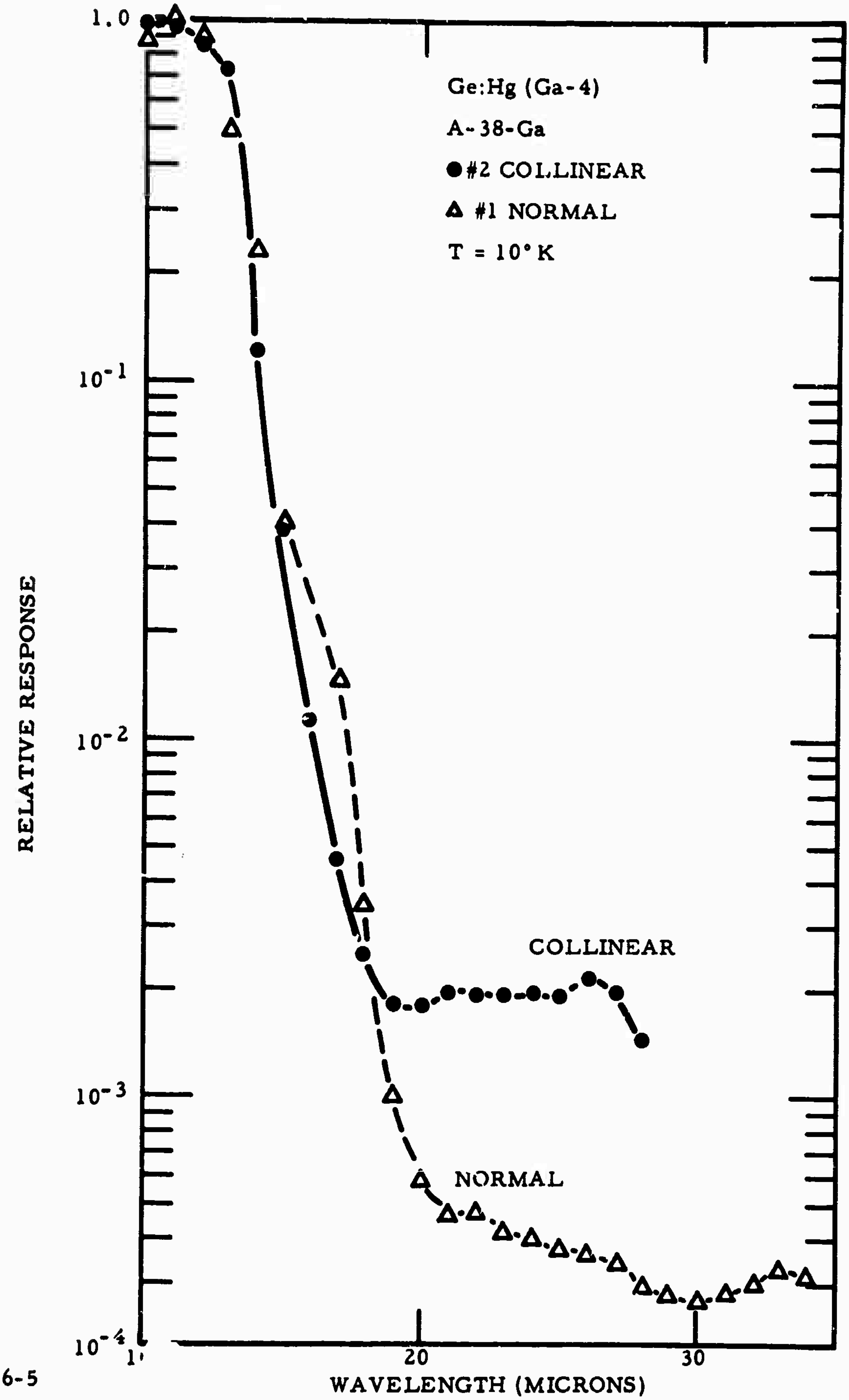

05066-5

Figure 5 Normal and Collinear Spectral Response for a Gallium-Diffused Layer Contact

TABLE I

Collinear and Normal Detector Response in a Signal Field of 1.2×10^{-5} Watt/Cm^2

Crystal	Element Resistance	$\frac{\Delta I}{I} \times 10^4$				
		Normal		Collinear		Normal/ Collinear
		actual	average	actual	average	
Au-Ga Alloy (Ge:Hg)						
DB 1170	0.4 MΩ	0.32		0.24		
		0.32		0.22		
			0.32		0.23	1.4
4-4-B-56	10 kΩ	0.49		0.36		
		0.46		0.28		
			0.48		0.32	1.5
7-1-A-56	18 kΩ	0.67		0.56		
		0.71		0.53		
			0.69		0.55	1.3
Ga Diffusion (Ge:Cu)						
Ge:Cu-4	130 kΩ	1.2		1.1		
				0.98		
			1.2		1.0	1.2
					Average $\frac{N}{C}$ = 1.4	

resistances were identical, to measurement accuracies, and thus are not listed separately. This is taken to indicate that a significant fraction of the 300°K background radiation reached the elements through surfaces other than the one facing the entrance aperture.

The normal and collinear detector elements had identical geometries; the mounting orientation determined whether the units were operated in the collinear or the normal mode (note Figure 3). Since the radiation absorbed will be largest in the first millimeter of the detector element, the collinear mode signal will be largest unless absorption in the contact layer reduces the signal. Thus, the average value of normal/collinear = 1.4 indicates a loss of at least 30% in the contact.

Contact resistance values were determined by measuring the resistance across two small contact points approximately 4 mm apart. Resistance values were approximately 7 ohms near 10°K.

The collinear and normal modes will be compared again in a later part of the report, but no significant differences in operating characteristics have been noted.

B. Alignment Requirements for Heterodyning

The discussion of heterodyning previously in this report assumed that the local oscillator signal and the incoming signal are perfectly aligned. Ross[1] gives an expression for the falloff of signal with misalignment angle θ as follows:

$$\frac{\text{Signal for } \theta = \theta}{\text{Signal for } \theta = 0} = \text{phi} = \frac{\sin(\beta \ell/2)}{(\beta \ell/2)}$$

where $\beta = \frac{2\pi}{\lambda_r} \sin\theta$. In this expression λ_r is the wavelength of the radiation and ℓ is the dimension of the detector being employed.

This expression was computer-calculated and is plotted in Figure 6. The data are for 10.6-micron radiation falling on detectors of varying dimensions ℓ. The situation described here is depicted in the insert of the figure. Note the critical angular tolerance; for a 1 mm detector the 50% falloff point is 0.36°. The alignment criterion is very severe for large detectors, indicating a practical necessity to use small detectors.

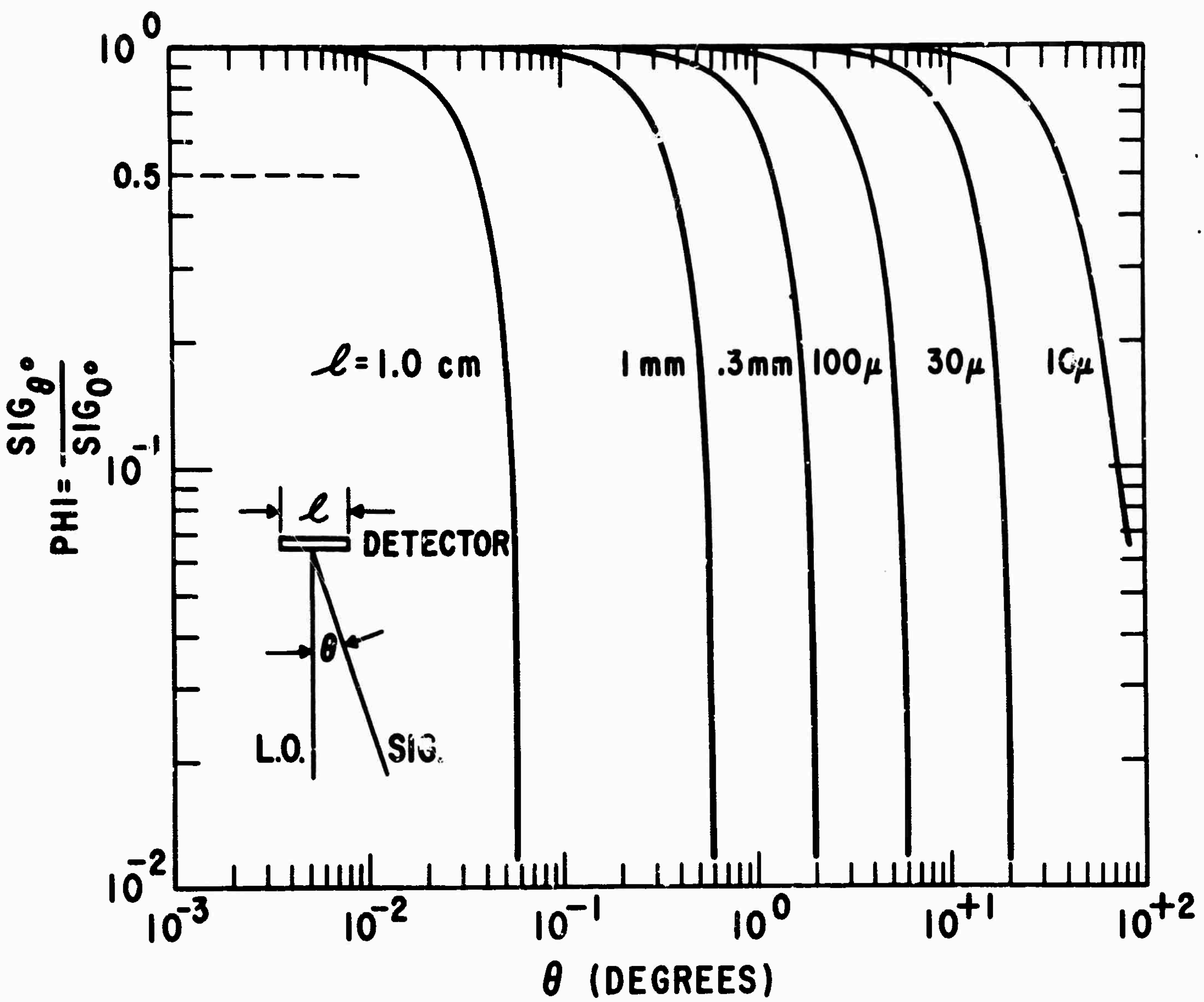

Figure 6 Falloff in Signal Response with Angular Misalignment of Signal and Local Oscillator Propagation Directions. The calculated curves are for 10.6 micron radiation and various one-dimensional detector dimensions given by each curve.

SECTION II

MATERIAL PROPERTIES

A. Dielectric Relaxation Studies

1. Introduction

A recent publication has shown[6] that a photoconductor has a component of the response time given by the dielectric relaxation (DR) time $\tau_\rho = \epsilon\rho/4\pi$ (ρ = resistivity and ϵ = dielectric constant). A continuing study of this phenomenon has demonstrated that for a given material there is a voltage above which the greater portion of the signal has a response time τ_ρ, while below that voltage the DR effects are secondary. At this voltage the drift length of the holes in Ge:Hg and Ge:Cu is of the order of the electrode separation. Details of the phenomenon follow.

2. Experimental

The experimental arrangement used for measuring detector element response times under reduced background conditions is identical to that utilized previously.[7] Since resistivity rather than temperature has been found to determine the DR effect, the data to be presented were taken near helium temperatures. No different results were observed when the temperature was increased.

Figure 7 illustrates the variation of the response time form as a function of increasing bias. At low voltages the signal is principally fast, but as the bias increases, the long time constant dominates. Figure 8 is based on data from pictures such as those in Figure 7. In Figure 8 the ordinate scale is the ratio of that part of the signal having a response time τ_ρ to the portion that is fast, i.e. A_ρ/A_f. This figure presents data from Ge:Hg crystals having a wide variety of sensitivities. The number in parentheses by each curve is the resistance of the element when it was

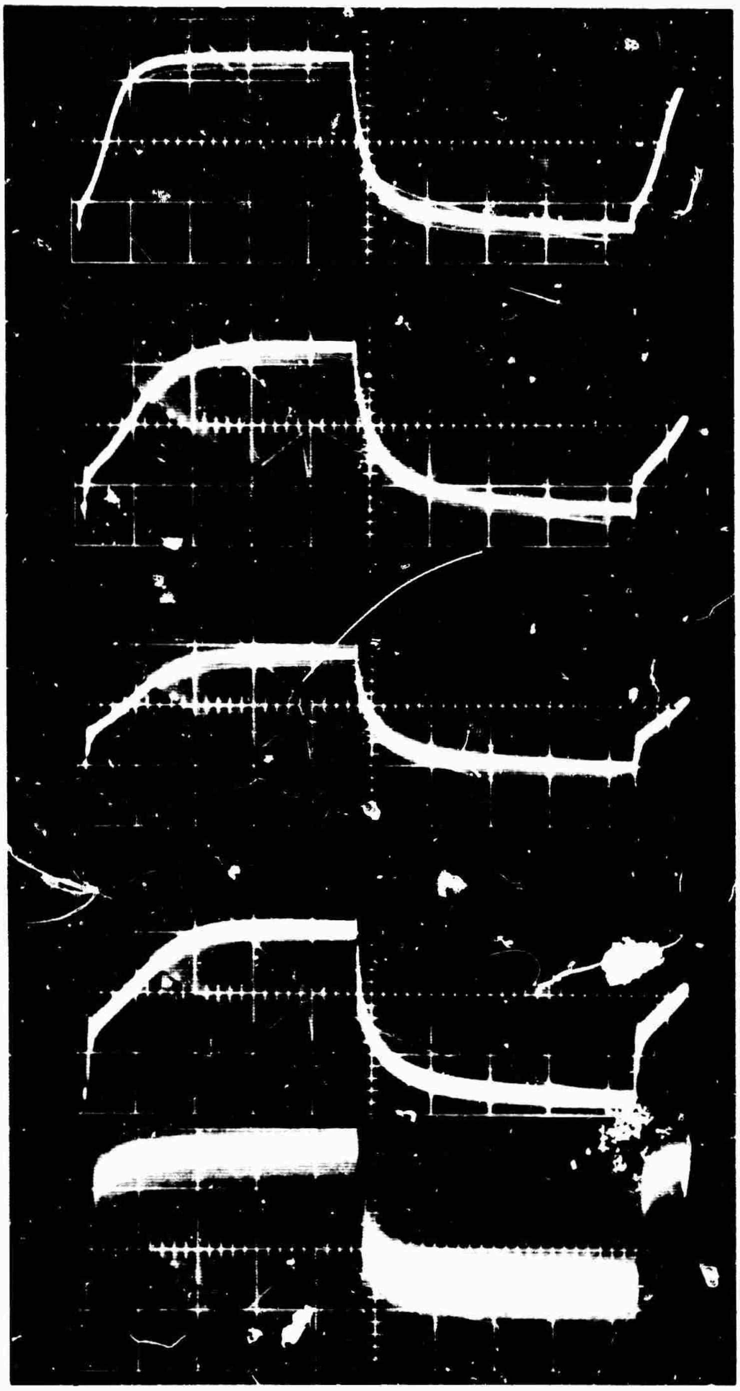

45V 10 μsec/cm

23V 10 μsec/cm

12V 10 μsec/cm

6V 5 μsec/cm

1.5V 5 μsec/cm

5158-10

Figure 7 Photographs of Oscilloscope Traces Showing the Change from Fast to Slow Signal Response as the Detector Bias Is Increased. The number to the left of each curve is the bias used when the data were taken. Detector resistance was 8 megohms; temperature was about 5°K.

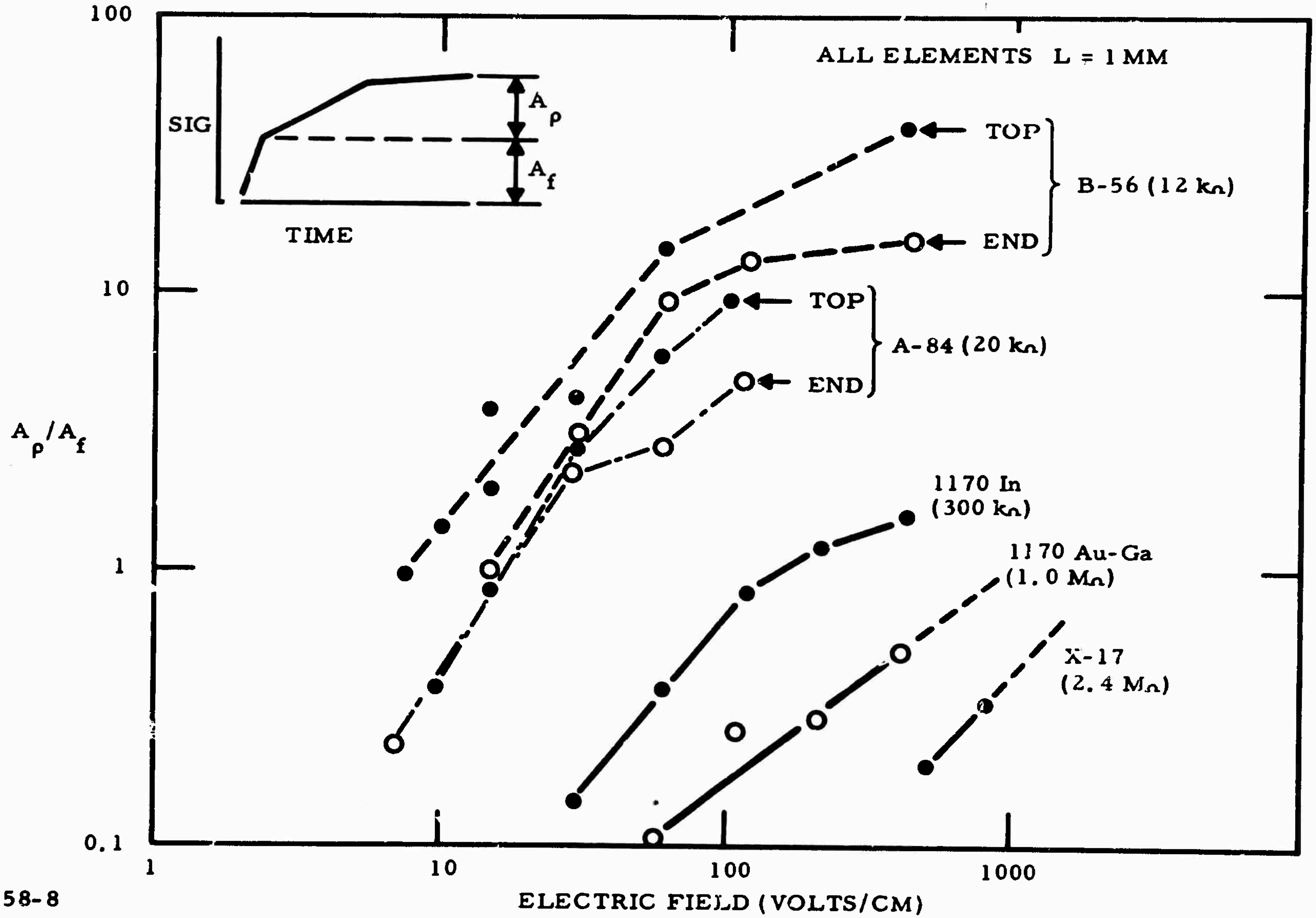

5158-8

Figure 8 Variation of A_ρ/A_f (see inset) with Electric Field for Detector Materials of Varying Sensitivities. The number in parentheses by each curve is the resistance of the detector when it is exposed to a 180° field-of-view, 300°K background radiation. The field required to reach the value of $A_\rho/A_f = 1$ increases with loss of material sensitivity. Similar results are obtained when the radiation is incident through contacts (tops) or through end of sample (end) (collinear versus normal).

operated exposed to 300°K background radiation. The field required to realize $A_p/A_f = 1$ (E_{DR}) increases as the sensitivity of the material falls off (higher resistance in 300°K background).

Figure 9 shows that the above low sensitivity - high E_{DR} correlation exists for other materials. The materials tested included Ge:Cu and Ge:Hg which had varying ratios of Cu to Hg concentration. It had been noted that Ge:Cu required much higher voltages than Ge:Hg before the DR time constants were observed. To determine if this fact was related to features of the Cu (e.g., its very high diffusion coefficient), Cu was added by diffusion to Ge:Hg in increasing amounts up to a concentration 10 times that of the Hg. Data for Ge:Hg without Cu, the same Ge:Hg with varying amounts of Cu diffused in, and Ge:Cu are plotted in Figure 9. The striking feature is that again, as with Ge:Hg, E_{DR} correlates (for $A_p/A_f = 1$) roughly with the 300°K background determined resistance of the samples, i.e., as the inverse of the sensitivity of the material.

From the two sets of data in Figures 8 and 9 it is clear that E_{DR} varies as the resistivity of the detector elements. Since for background controlled conditions $R \propto 1/Q_B \eta \mu \tau$, then E_{DR} must be inversely proportional to the $\mu\tau$ product.

a. Field Dependence

To establish if the effects were purely field-dependent, samples were were cut in various thicknesses and E_{DR} was determined. The set of curves in Figure 10 was obtained by recutting and grinding the same elements to produce first 3 mm, then 1 mm, and finally 0.3 mm electrode separation. The electrode shape was 1 mm x 6 mm in all cases. It is clear that the E_{DR} values increase with sample thickness roughly in proportion to the electrode separation L.

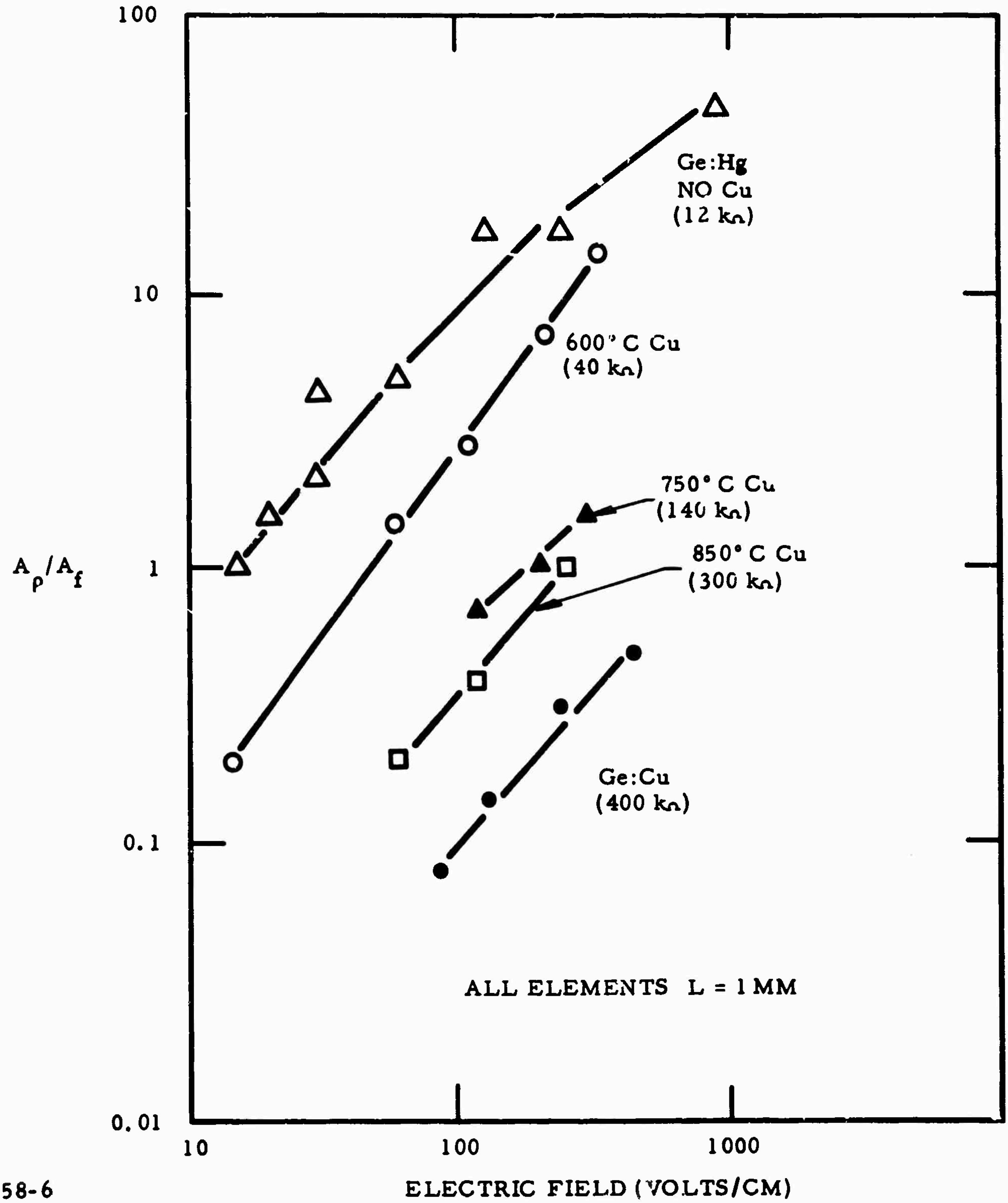

5158-6

Figure 9 Variation of A_ρ/A_f with Electric Field for Ge:Hg, Ge:Cu, and Mixed Ge:Hg:Cu Materials. Copper was added to Ge:Hg materials by diffusions at 600°C, 750°C, and 850°C (10^{14}, 10^{15}, and 10^{16} copper atoms/cc respectively). The photographs of Figure 7 show the 600°C diffusion material.

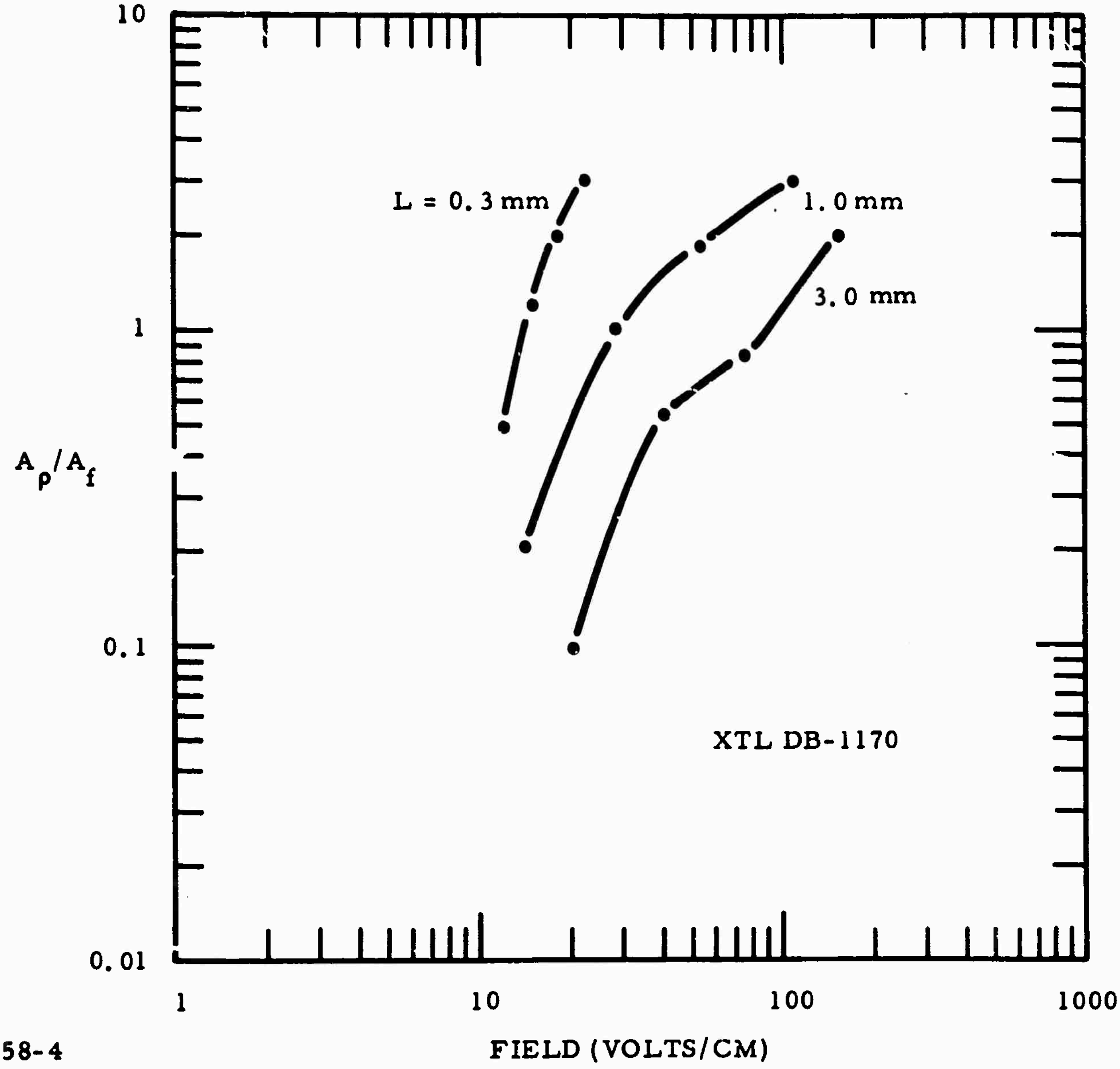

5158-4

Figure 10 Variation of the Field Dependence of the DR Effects with Electrode Separation. From data such as these in the graph the onset of DR effects is shown to require fields roughly proportional to the electrode spacing.

Since $E_{DR} \propto L$ and $E_{DR} \propto 1/\mu\tau$, it is clear that we are observing an effect associated with the drift distance, $S = \mu E\tau$, with the dielectric relaxation effects coming in with S of the order of L. Using a μ value of 1.0×10^5 cm^2/V-sec, a lifetime of 10^{-7} sec, and L = 1.0 mm gives an E_{DR} of 10 volts per cm. Such a lifetime is representative of crystal A-84, which has an E_{DR} value of 15 to 20 V/cm (see Figure 8). Thus, a crystal such as X-17 with a short lifetime (or at least a short $\mu\tau$ product) will require high fields before S becomes comparable to L. In addition, as the electrode spacing increases, E must increase to increase S to the larger L value.

b. Field Dependence o Other Parameters

In addition to the above field onset phenomenon, sensitivity variations occur for electric field values in the vicinity of E_{DR}. Figure 11 contains sensitivity and resistance data versus bias. The photoconductive current for a fixed signal is divided by the applied bias and plotted versus bias. With such a plot deviations from a horizontal line indicate nonlinearities. It is clear that the current responsivity increases in the vicinity of $A_p/A_f = 1$; the A_p/A_f data are plotted on the same graph for ease of comparison. Also, the resistance of the Ge:Hg element falls in the same bias range as the responsivity. This is expected because the resistance is a direct current measurement of the inverse of the sensitivity of the element to the background radiation, $I_{DC}/V \propto \mu\tau Q_B$.

As an extension of the above argument, the detector's open circuit voltage would not show the variation seen in Figure 11, because the $\mu\tau$ values of the signal current factor cancel with the $1/\mu\tau$ factor of the detector resistance. By the same argument, i_S/I_{DC} plots do not reveal the variations of Figure 11.

It should be noted that the sensitivity versus bias data compiled in Figure 11 were taken with the element resistance nearly 3 orders of magnitude smaller than when the DR effects were taken; yet the field for the onset

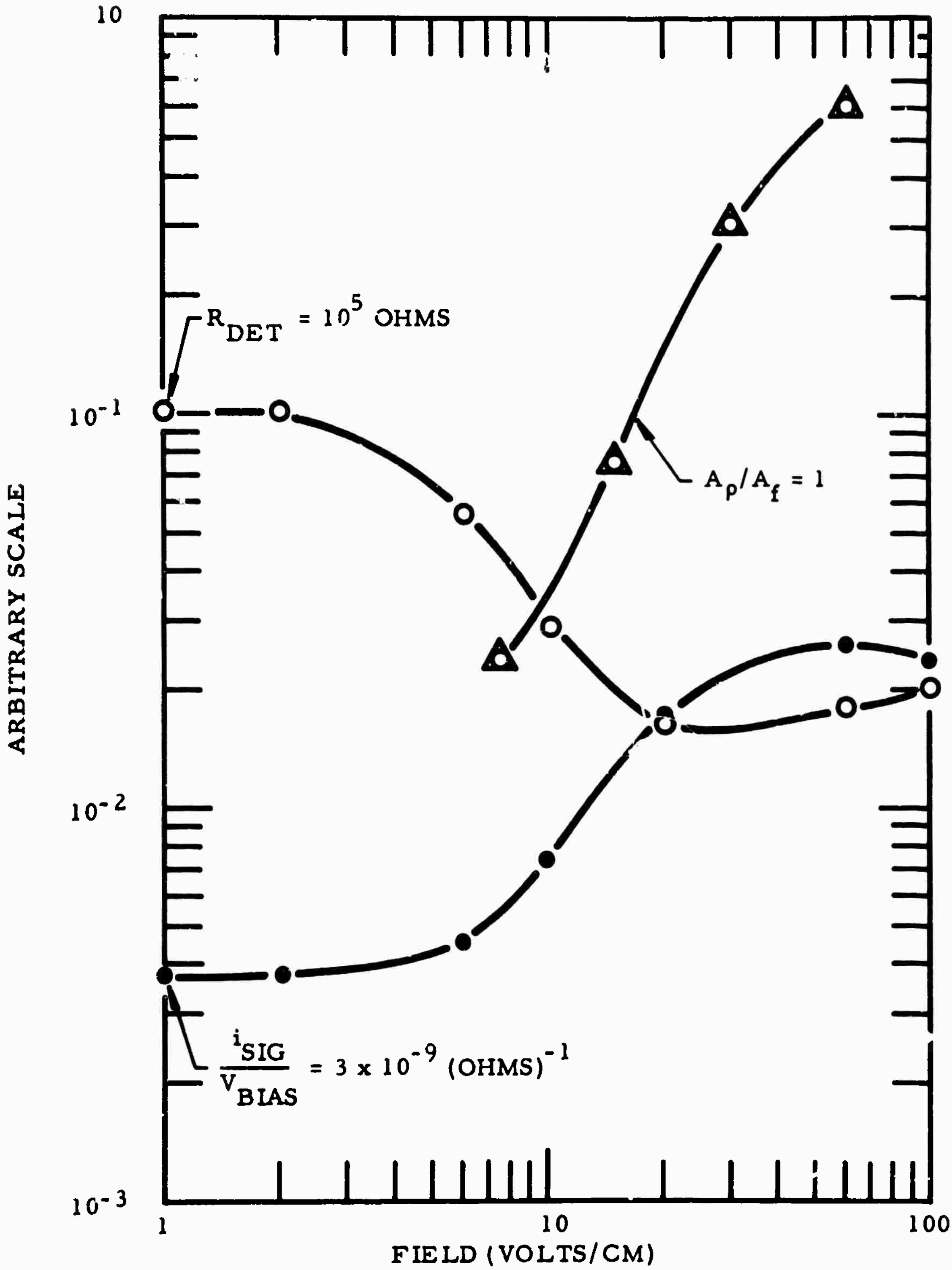

5158-7

Figure 11 Variation of Current Responsivity i_S/V, Detector Resistance, and A_ρ/A_f with Electric Field. It is apparent that changes in each of the parameters occur across the same field region. Note that the responsivity increases with field as it does in all cases. Temperature of operation is ~ 10°K.

of the various effects remains the same. Such behavior is consistent with there being no lifetime change in the range of resistivities from 10^5 to 10^9 ohm-cm.

c. Saturation of the Fast Component

Another aspect of the DR phenomenon is shown in Figure 12. At biases substantially above E_{DR} it is difficult to accurately ascertain the value of A_f. To better evaluate the change of A_f with bias, the signal was measured versus bias at several frequencies. The data were taken using an InAs diode light source and varying the driving frequency square wave current. Reduced background conditions were utilized so that reasonable frequencies would be substantially above $1/\tau_\rho$.

The 15 Hz curve is a total, fast plus slow, response curve and shows the superlinearity seen for devices near E_{DR}. At the higher frequencies a saturation of the signal is seen. The small turnup at the higher biases for the 15 kHz curve occurs from the increasing low frequency signal This arises as the signal has the form

$$S = \frac{A_\rho(E)}{(1 + \omega^2\tau_\rho^{\,2})^{\frac{1}{2}}} + \frac{A_f(E)}{(1 + \omega^2\tau_f^{\,2})^{\frac{1}{2}}} \quad .$$

At 15 kHz this reduces to

$$S = \frac{A_\rho(E)}{\omega\tau_\rho} + A_f \quad .$$

With increasing bias, after A_f has saturated, the increasing first term will eventually be detected. By going to a still higher frequency, 150 kHz, the first term is reduced to negligible values even at the highest biases employed.

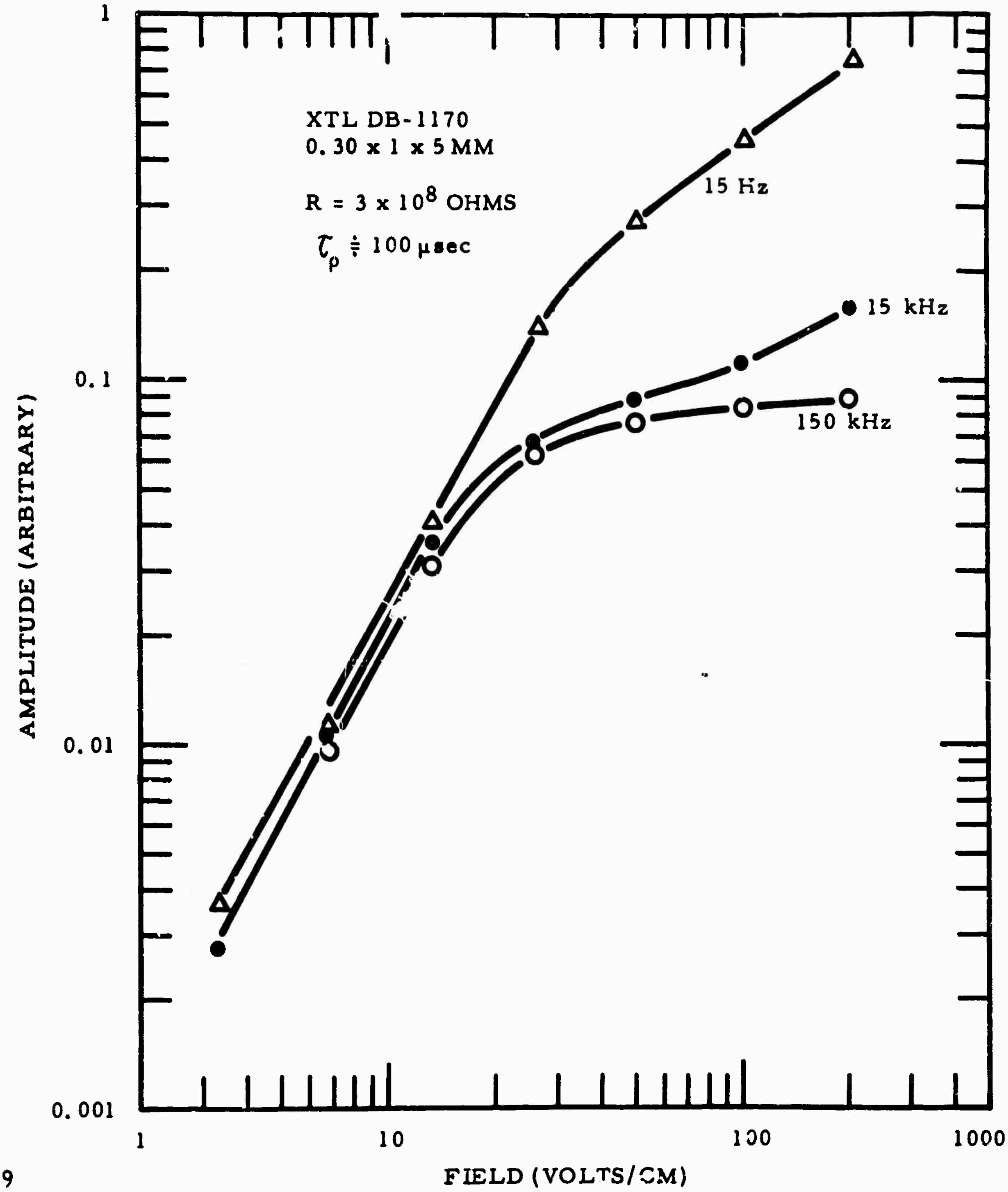

5158-9

Figure 12 Variation of the Total Signal, 15 Hz, and the Fast Component, 15 kHz and 150 kHz, with Bias. By using higher frequencies the large slow component can be removed from the measurement.

For comparison with this detector element, $A_p/A_f = 1$ for $E = 15$ V/cm. (See Figure 10.) For this experiment the resistivity of the element was 2×10^8 ohm-cm and τ_p was 1.0×10^{-4} second.

3. Discussion of Results

The results obtained are explained with the aid of the schematic diagram of the detector geometry (Figure 13). Consider the situation when the drift length S is a fraction of the electrode spacing L. On the average, holes generated by the background and signal radiation absorbed in a distance S from the positive electrode will drift out of this region before recombining. On the other hand, recombination will occur in this same region with holes coming from the electrode. As S increases with bias, that portion of the crystal dependent on the electrode supply of holes for recombination increases until S ≥ L when all the recombination is taking place with holes originating from the electrode. Thus, it appears that quite different conditions must prevail regarding the hole supply or current flow pattern when all the recombination is with electrode-supplied holes.

With present contacting procedures, no deviation from linearity of the I-V characteristics nor any significant polarity dependence has been observed. It appears that if the contacts play a role, it must involve subtle details of the contact structure.

The possibility must be considered that the effects are primarily bulk effects, i.e., the contact is more uniform than the bulk and the difference in performance arising when S becomes comparable to L occurs because the electrode supplies charge uniformly, while the bulk nonuniformities require a particular current flow pattern.

Various explanations for the DR effects are being explored.

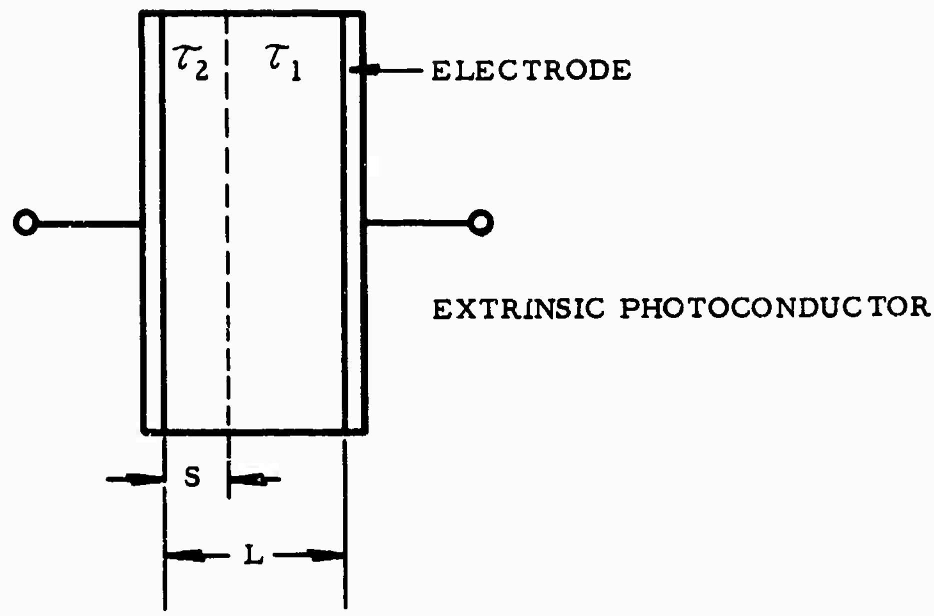

5158-10

Figure 13 Schematic Diagram of a Detector. From the responsivity data it is apparent that the lifetime near the positive electrode (hole supply electrode) must be greater than in the region farther from the electrode than S ($\tau_2 > \tau_1$).

B. Impurity Interactions

1. Gettering of Copper with a Gallium-Diffused Layer

In the preparation of Ge:Hg crystals the presence of unwanted impurities is detected through the study of the resistance (or Hall coefficient) - temperature characteristics. In Figure 14 the resistance of a detector element is plotted against reciprocal temperature. The curve labelled "Original" has a slope indicating an activation energy of 0.039 eV. This is less than half the value expected from mercury impurities which have an ionization energy of 0.088 eV. The deviation arises because of the presence of residual p-type impurities whose concentration is such that the Fermi level is located below the Hg level.

In the course of studies of gallium-diffused layers on Ge:Hg elements, an increase in the activation energy was noted. Further study indicated that a gallium diffusion followed by a short anneal substantially increases the activation energy of materials which originally had values in the 0.04 to 0.06 range.

The simple explanation of this result is that the gallium-diffused layer is a region in which copper is highly soluble; thus, the diffused layer getters copper from the crystal. There are two reasons for high solubility in the diffused layer, electronic and pairing enhancement.

2. Electronic Solubility Enhancement

The presence of the high acceptor concentration increases the solubility because of charge considerations by a factor N_A/n_i over the high purity solubility N_o^+.[7] The two curves N_o^+ and $N_o^+ \times 10^{20}/n_i$ of Figure 15 indicate the solubility enhancement expected for an acceptor concentration $N_A = 10^{20}/cc$.

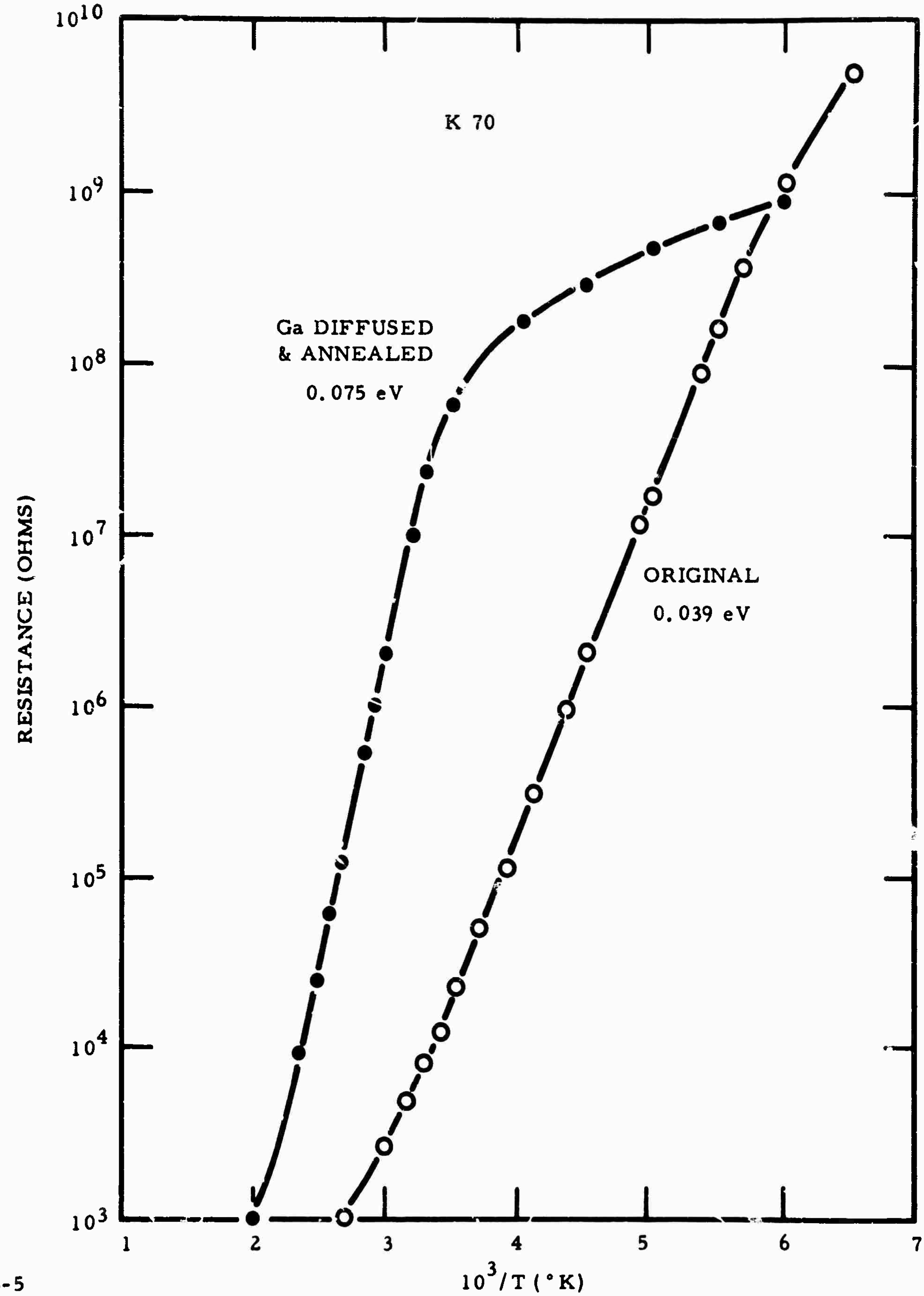

5158-5

Figure 14 Impurity Gettering with a Gallium-Diffused Layer. By diffusing gallium into the surface of Ge:Hg, then annealing, impurities are removed. An improved resistance temperature characteristic results. (0.039 eV activation energy increased to 0.075 eV.)

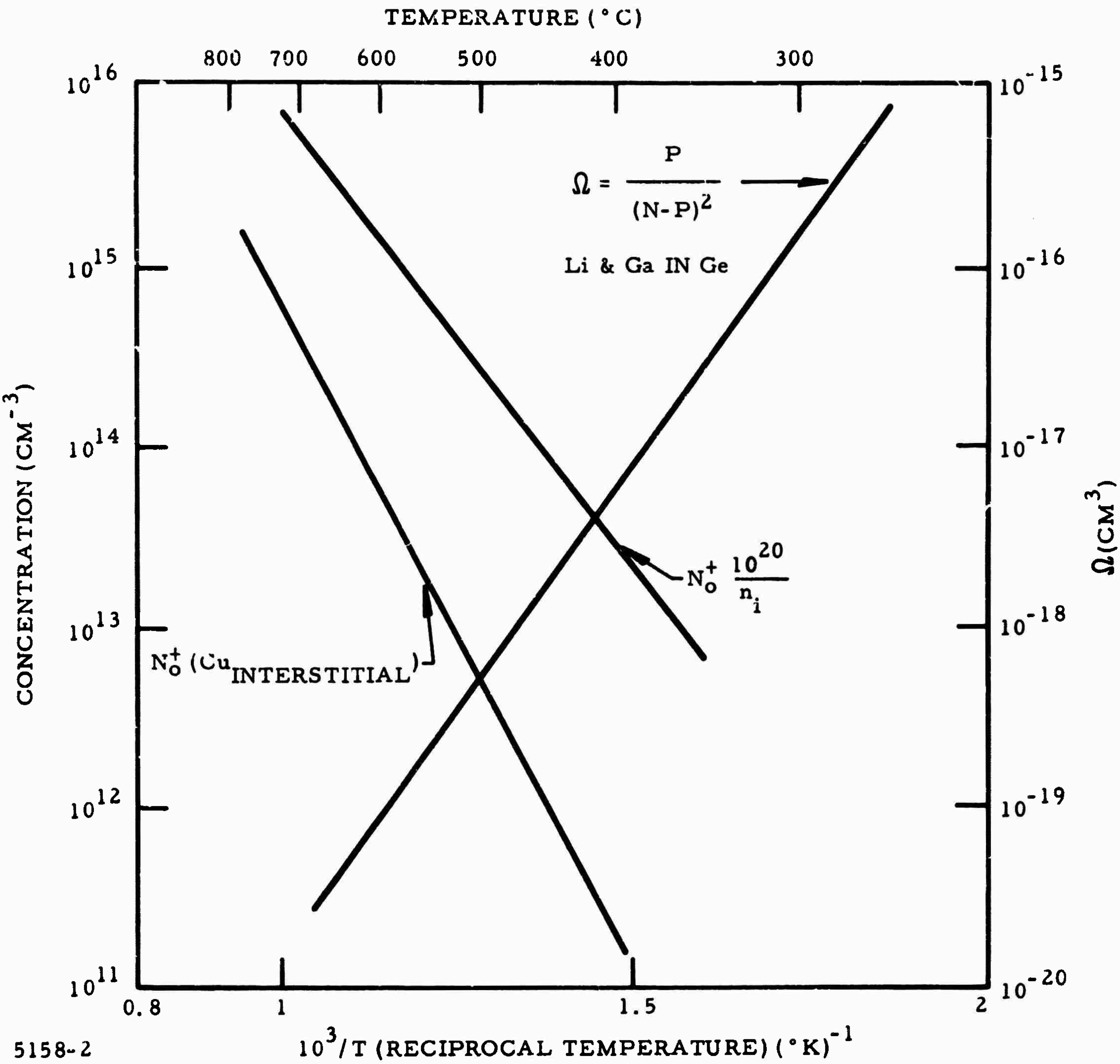

5158-2

Figure 15 Solubility Enhancement due to Acceptors. N_o^+ high purity Cu donor solubility, $N_o \times 10^{20}/n_i$ solubility in presence of 10^{20} acceptor atoms (electronically enhanced), Ω the fraction of Li and Ga atoms paired in Ge (solubility enhanced as pairing increases).

3. Pairing Solubility Enhancement

Pairing of acceptor gallium atoms with donor copper atoms results in the takeup of copper by the diffused layer. The third curve of Figure 15, labelled "Ω", is the fraction of Li ions paired with Ga ions in Ge. This is calculated data of Reis, Fuller, and Morin.[8] This curve is plotted only to show that pairing solubility is greatly enhanced at low temperatures, while electronic solubility is greatest at highest temperatures.

4. Radioactive Copper

Preliminary data taken using radioactive Cu-64 has confirmed that copper is gettered into the diffused layer, but no details of the mechanism have yet been established.

REFERENCES

1. M. Ross, Laser Receivers (John Wiley and Sons, New York, 1966).
2. M. C. Teich, R. J. Keyes, and R. H. Kingston, Appl. Phys. Letters 9, 357 (1966).

   C. S. Bucjek and G. S. Picus, Appl. Phys. Letters 11, 125 (1967).
3. R. A. Soref, Electronic Letters 2, 410 (1966).
4. H. A. Gebbie, N.W.B. Stone, E. H. Putley, and N. Shaw, Nature 214, 165 (1967).
5. R. L. Williams and B. H. Breazeale, Phys. Rev. Letters 25, 1129 (1967).
6. R. L. Williams, J. Appl. Phys. 38, 4802 (1967).
7. R. N. Hall and J. H. Racette, J. Appl. Phys. 35, 379 (1964).
8. H. Reiss, C. S. Fuller, and F. J. Morin, Bell System Tech. J. 35, 535 (1956).

Unclassified
Security Classification

DOCUMENT CONTROL DATA - R&D

(Security classification of title, body of abstract and indexing annotation must be entered when the overall report is classified)

1 ORIGINATING ACTIVITY (Corporate author) Texas Instruments Incorporated 13500 North Central Expressway Dallas, Texas 75222	2a. REPORT SECURITY CLASSIFICATION Unclassified 2b GROUP -

3 REPORT TITLE

High-Speed, Long-Wavelength Coherent Radiation Detectors

4. DESCRIPTIVE NOTES (Type of report and inclusive dates)
Semiannual Technical Summary Report, 15 May 1967 through 15 November 1967

5 AUTHOR(S) (Last name, first name, initial)

Williams, R. L.

6. REPORT DATE	7a. TOTAL NO. OF PAGES	7b. NO. OF REFS
December 1967	36	8

8a. CONTRACT OR GRANT NO. N00014-67-C-0497 b. PROJECT NO. ARPA Order No.: 269, Amendment No. 13 c. Program Code: 7E30 d	9a. ORIGINATOR'S REPORT NUMBER(S) 08-67-90 9b. OTHER REPORT NO(S) (Any other numbers that may be assigned this report)

10 AVAILABILITY/LIMITATION NOTICES

Reproduction in whole or in part is permitted for any purpose of the United States Government.

11. SUPPLEMENTARY NOTES	12. SPONSORING MILITARY ACTIVITY Office of Naval Research, Washington, D.C. in cooperation with Advanced Research Projects Agency, Washington, D.C.

13 ABSTRACT

The principal consideration in the heterodyne mode of signal detection is the influence of the local oscillator power on detector characteristics. It is shown that misalignment of the local oscillator signal can seriously degrade detection performance with the detector geometry presently used. For signals incident through transparent contacts, misalignment problems are removed. Characteristics of transparent contacts are reported.

It has been established that dielectric relaxation time constant effects occur above a certain electric field. These effects, as well as nonlinearities of signal and detector resistance changes, occur at fields for which the drift length of holes is comparable to the electrode separation. This has been shown to be valid by examining detectors having different thicknesses and material having a wide range of carrier lifetimes.

Mercury-doped germanium samples which have been subjected to gallium diffusions have larger activation energies than untreated material. This change has been identified with copper gettering by the gallium-diffused surface layer.

DD FORM 1 JAN 64 1473

Unclassified
Security Classification

14 KEY WORDS	LINK A		LINK B		LINK C	
	ROLE	WT	ROLE	WT	ROLE	WT
photoconductivity in Ge:Hg and Ge:Cu						
conditions for heterodyne detection						
response times limited by dielectric relaxation						
responsivity changes with electric field						
field dependent carrier lifetime						
gettering of copper from Ge:Hg						

INSTRUCTIONS

1. ORIGINATING ACTIVITY: Enter the name and address of the contractor, subcontractor, grantee, Department of Defense activity or other organization *(corporate author)* issuing the report.

2a. REPORT SECURITY CLASSIFICATION: Enter the overall security classification of the report. Indicate whether "Restricted Data" is included. Marking is to be in accordance with appropriate security regulations.

2b. GROUP: Automatic downgrading is specified in DoD Directive 5200.10 and Armed Forces Industrial Manual. Enter the group number. Also, when applicable, show that optional markings have been used for Group 3 and Group 4 as authorized.

3. REPORT TITLE: Enter the complete report title in all capital letters. Titles in all cases should be unclassified. If a meaningful title cannot be selected without classification, show title classification in all capitals in parenthesis immediately following the title.

4. DESCRIPTIVE NOTES: If appropriate, enter the type of report, e.g., interim, progress, summary, annual, or final. Give the inclusive dates when a specific reporting period is covered.

5. AUTHOR(S): Enter the name(s) of author(s) as shown on or in the report. Enter last name, first name, middle initial. If military, show rank and branch of service. The name of the principal author is an absolute minimum requirement.

6. REPORT DATE: Enter the date of the report as day, month, year; or month, year. If more than one date appears on the report, use date of publication.

7a. TOTAL NUMBER OF PAGES: The total page count should follow normal pagination procedures, i.e., enter the number of pages containing information.

7b. NUMBER OF REFERENCES: Enter the total number of references cited in the report.

8a. CONTRACT OR GRANT NUMBER: If appropriate, enter the applicable number of the contract or grant under which the report was written.

8b, 8c, & 8d. PROJECT NUMBER: Enter the appropriate military department identification, such as project number, subproject number, system numbers, task number, etc.

9a. ORIGINATOR'S REPORT NUMBER(S): Enter the official report number by which the document will be identified and controlled by the originating activity. This number must be unique to this report.

9b. OTHER REPORT NUMBER(S): If the report has been assigned any other report numbers *(either by the originator or by the sponsor)*, also enter this number(s).

10. AVAILABILITY/LIMITATION NOTICES: Enter any limitations on further dissemination of the report, other than those imposed by security classification, using standard statements such as:

(1) "Qualified requesters may obtain copies of this report from DDC."

(2) "Foreign announcement and dissemination of this report by DDC is not authorized."

(3) "U. S. Government agencies may obtain copies of this report directly from DDC. Other qualified DDC users shall request through ________________."

(4) "U. S. military agencies may obtain copies of this report directly from DDC. Other qualified users shall request through ________________."

(5) "All distribution of this report is controlled. Qualified DDC users shall request through ________________."

If the report has been furnished to the Office of Technical Services, Department of Commerce, for sale to the public, indicate this fact and enter the price, if known.

11. SUPPLEMENTARY NOTES: Use for additional explanatory notes.

12. SPONSORING MILITARY ACTIVITY: Enter the name of the departmental project office or laboratory sponsoring *(paying for)* the research and development. Include address.

13. ABSTRACT: Enter an abstract giving a brief and factual summary of the document indicative of the report, even though it may also appear elsewhere in the body of the technical report. If additional space is required, a continuation sheet shall be attached.

It is highly desirable that the abstract of classified reports be unclassified. Each paragraph of the abstract shall end with an indication of the military security classification of the information in the paragraph, represented as *(TS)*, *(S)*, *(C)*, or *(U)*.

There is no limitation on the length of the abstract. However, the suggested length is from 150 to 225 words.

14. KEY WORDS: Key words are technically meaningful terms or short phrases that characterize a report and may be used as index entries for cataloging the report. Key words must be selected so that no security classification is required. Identifiers, such as equipment model designation, trade name, military project code name, geographic location, may be used as key words but will be followed by an indication of technical context. The assignment of links, rules, and weights is optional.